



## **Navigation Demonstrations of Precision Ranging with the Ulysses Spacecraft**

T.P. McElrath  
S.W. Thurman  
K.E. Criddle

Jet Propulsion Laboratory  
California Institute of Technology  
Pasadena, CA

# **AAS/AIAA Astrodynamics Specialist Conference**

**VICTORIA, B. C., CANADA AUGUST 16-19, 1993**  
**AAS Publications Office, P.O. Box 28130, San Diego, CA 92198**

## NAVIGATION DEMONSTRATIONS OF PRECISION RANGING WITH THE ULYSSES SPACECRAFT

T. P. McElrath\*  
S. W. Thurman\*\*  
K. E. Criddle†

Radio tracking data acquired from the Ulysses spacecraft during its flight to Jupiter were used to test experimental navigational techniques for processing highly accurate (1 to 2 m) two-way ranging data. While ranging data with this level of accuracy have been routinely used for navigation of Earth-orbiting spacecraft, ranging data from interplanetary spacecraft have in the past been artificially deweighted to accuracies of 100 to 1000 m, due to difficulties in modeling ground station and transmission media calibration errors and small spacecraft non gravitational forces. This paper describes the incorporation of a simple model of solar plasma-induced variations in ranging data into a procedure for reducing ranging data taken near conjunction with an assumed accuracy near the inherent accuracy of the measurements. Application of this model to Ulysses ranging data acquired at either S-band (2.3 GHz) or X-band (8.4 GHz) frequencies is shown to permit effective utilization of single-band data over Sun-spacecraft separation angles down to 2 degrees.

### INTRODUCTION

Although ranging data with accuracies of a few meters have been frequently used for navigation of Earth-orbiting spacecraft, the use of this data type in interplanetary navigation, with data arcs spanning weeks or months, was often accomplished in the past by artificially deweighting the data to accuracies of 1000 meters or more, because of difficulties in modeling the day-to-day variability of ground station calibration errors, transmission media calibration errors, and small, random spacecraft non gravitational forces. Relatively recent attempts to develop models for these error sources that permit ranging data with accuracies of a few meters to be fully utilized have been successful in demonstrations performed with both the

---

\* Ulysses Navigation Team Leader, Member Technical Staff, Navigation Systems Section, Jet Propulsion Laboratory, California Institute of Technology, Pasadena, California 91109.

\*\* Technical Manager, Navigation Systems Section, Jet Propulsion Laboratory, California Institute of Technology, Pasadena, California 91109; Member AAS.

† Member of the Professional Staff, Sterling Software, Pasadena, California 91109.

Galileo and Ulysses spacecraft (Refs. 1-4). The results obtained in these experiments indicated that with sufficient accuracy, ranging data acquired from widely separated ground stations possess a radio direction-finding capability that can approach that of more sophisticated, but complex, data types based on Very Long Baseline Interferometry (VLBI) techniques.

This paper describes an extension of the data reduction technique developed in the previous experiments to include an approximate model for the effect of charged particles in the solar plasma on range measurements. The solar plasma effect can become the most significant error source affecting ranging data for small ( $< 45$  degree) Sun-spacecraft separation angles, so the inclusion of an explicit model for this effect is needed to process accurate ranging data over the widest possible range of separation angles from the Sun. The experiments described herein were conducted in conjunction with the Ulysses mission, which is a cooperative project of NASA and the European Space Agency. The Ulysses spacecraft is designed to measure the emissions from the poles of the Sun and the surrounding heliospheric environment. Following its launch in October 1990, Ulysses obtained a gravity assist from Jupiter on February 8, 1992, which rotated its orbit plane 80 degrees out of the ecliptic plane, allowing the spacecraft to spend a total of 234 days over the South and North polar regions of the Sun in 1994 and 1995.

The Ulysses radio system normally operates with an S-band uplink frequency (2.1 GHz) and an X-band downlink frequency (8.4 GHz), although an S-band downlink (at 2.3 GHz) is available when needed. The radio system includes a transponder to support two-way, coherent Doppler and range measurements, as well as the modulation and demodulation of science and engineering telemetry data. Tracking, telemetry, and command operations with the spacecraft are conducted by the ground stations of the NASA /JPL Deep Space Network (DSN). Doppler and ranging data acquired from Ulysses have exhibited noise levels of about 0.2 mm/s and 1 to 2 m, respectively, approaching the performance of an X-band uplink/X-band downlink (X/X) tracking system, even though Ulysses employs an S-band uplink, which is much more sensitive to charged particle phenomena. In addition to the two-way Doppler and ranging data, VLBI data have also been obtained from Ulysses at X-band frequencies during certain periods, by configuring the spacecraft's radio signal spectrum appropriately.

Ulysses experienced its first solar conjunction in August 1991, around which time tracking data were acquired from the spacecraft at Sun-spacecraft separation angles as small as 1.42 degrees. It is this data set which provides the basis for testing the accuracy and utility of the approximate solar plasma delay model which has been proposed for processing ranging data acquired under these conditions. The model is tested by estimating the solar plasma behavior as the spacecraft approached conjunction using different subsets of the Ulysses ranging and Doppler data, and by examining the consistency of solutions for the spacecraft trajectory computed from these different subsets in conjunction with the Doppler and VLBI data sets.

## SOLAR PLASMA MODELLING

A simple and well-known approximation of the solar plasma stream emanating from the Sun is to assume that the electron density at any given point is inversely proportional to the square of the distance to the Sun, as specified in Eq. (1), where  $\rho$  is the electron density,  $r$  is the distance from the Sun, and  $N$  is a field strength parameter with units of electrons per distance.

$$\rho = \frac{N}{r^2} \quad (1)$$

When determining the range delay due to total electron content on the signal path, the parameter  $N$  in Eq. (1), can be replaced by a scaling factor  $a$  which relates range delay and signal length. Interplanetary spacecraft operated by NASA and ESA normally use frequencies in the S-band, between 2.1 and 2.3 GHz or in the X-band, between 7.1 and 8.4 GHz. Representative values of  $a$  are  $1.672 \times 10^9 \text{ km}^2$  for S-band and  $1.232 \times 10^8 \text{ km}^2$  for X-band, respectively, given by Coles and Harmon.<sup>5</sup>

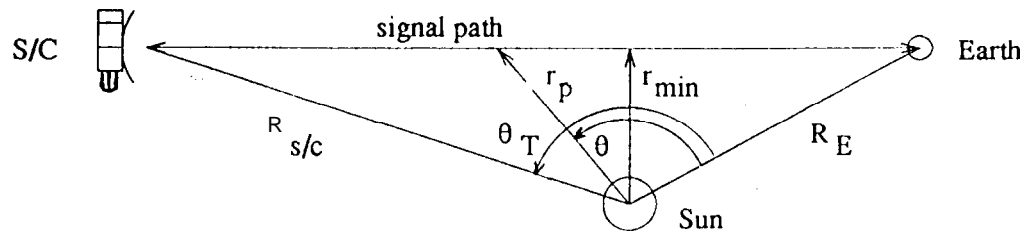


**Figure 1 Geometric quantities used to derive the solar plasma model.**

The effect of charged particles (electrons) on range data is to introduce a delay that is proportional to the number of particles encountered along the signal path from the Earth to the spacecraft. For this model the total range delay  $D$  along this path is given by the line integral shown in Eq. (2), where  $r_p$ , the Sun-signal distance evaluated along the signal path, is given in Eq. (3). In Eq. (3),  $R_{min}$  is the minimum distance from the Sun to the signal path, and  $\theta$  is the angle subtended (at the Sun) between the Earth to the point at which  $r_p$  is to be evaluated, as shown in Figure 1 (along with the other geometric quantities used in this derivation. )

$$D = a \int_{\text{Earth}}^{\text{s/c}} \frac{ds}{r^2} \quad (2)$$

$$r_p = \frac{R_{min}}{\sin \theta} \quad (3)$$

The evaluation of the integral in Eq. (2) is given in Eq. (4), in which  $\theta_T$  is the Earth-Sun-spacecraft angle. The value of  $R_{min}$  is given by Eq. (5), in which  $R_{s/c}$  is

the Sun-spacecraft distance and  $R_E$  is the Sun-Earth distance. Similar expressions have been derived previously by Efron and Lisowski<sup>6</sup>, using the same assumptions that were used here.

$$D = \frac{a\theta_T}{R_{min}} \quad (4)$$

$$R_{min} = \frac{R_{s/c} R_E \sin \theta_T}{\sqrt{R_{s/c}^2 + R_E^2 - 2R_{s/c} R_E \cos \theta_t}} \quad (5)$$

In all, Eqs. (4) and (5) indicate that only four quantities determine the range delay: the scaling factor, the solar angle from the Earth to the spacecraft, and the solar distances of the Earth and the spacecraft. Equations (4) and (5), together with their partial derivatives with respect to the positions of the Earth and the spacecraft, provide the formulas needed to compute the expected value of the solar plasma delay in range measurements, and to estimate corrections to the modeled solar plasma values in the orbit determination process based on discrepancies between the predicted and observed values of range measurements.

## SPACECRAFT MODELLING AND ESTIMATION METHOD

The spacecraft trajectory and the trajectory partial derivatives with respect to the estimated parameters are numerically integrated through the data arc, taking into account the gravitational and non gravitational accelerations acting on the spacecraft. The gravitational accelerations of all the planets, the Moon, and the Sun are included, as is the relativistic acceleration due to the Sun. The non gravitational accelerations include the solar radiation pressure (SRP) acting on the spacecraft and spacecraft attitude maneuvers. Due to the complex shape of the Ulysses spacecraft, the SRP force is modelled as a tabular function of the angle between the spacecraft's spin axis and the Sun. A scaling constant for the whole SRP model is estimated, both as a time-varying and as a constant parameter. The spacecraft is spin-stabilized, resulting in a low level of attitude control perturbations to the spacecraft's trajectory, but precession maneuvers are still necessary every few days to keep the high gain antenna pointed at the Earth. In addition, a series of daily maneuvers were implemented during the two weeks closest to conjunction in order to point the spacecraft spin axis on an arc around the Sun, to avoid violating attitude constraints. Both sorts of maneuvers were modeled, but only their  $\Delta V$  magnitudes were estimated due to the precise pointing knowledge available from the Ulysses spacecraft. The last trajectory correction maneuver, TCM-3, occurred on July 8, 1993, and all three of the components of an impulsive  $\Delta V$  were estimated.

Parameters affecting the observations were also included in the estimation process. The effect of the Earth's ionosphere on the tracking data was modeled based on Faraday rotation data collected at the same time or a predicted model, and the troposphere was calibrated using a seasonal model. The effect of errors in the

troposphere and ionosphere calibrations are accounted for, as are the effect of the uncertainty in the locations of the DSN tracking stations. The spacecraft spin introduces a bias in the Doppler data, which is calibrated, but the calibration error is also estimated to remove the effect of small spin-rate errors. A range bias was estimated for each station pass to account for the effect of station delay calibration errors. Most of these models are described in more detail by McElrath *et al.*<sup>4</sup> The solar plasma model described above was applied to the ranging data and a correction to it was estimated as a percentage of the nominal modeled delay.

Table 1  
ESTIMATION MODELS

<u>Estimated Parameters</u>	<u>A priori Uncertainty</u>
Spacecraft position	$10^5$ km
Spacecraft velocity	$10^2$ km/sec
SRP constant coefficient	20 % of nominal model
TCM-3 components	10 cm/sec
precession maneuver $\Delta V$ 's	10 cm/sec
Conjunction attitude maneuver $\Delta V$ 's	5 mm/sec
Range biases	5 meters
<u>Estimated Stochastic Parameters</u>	
SRP time-varying coefficient (30 day time constant)	10 % of nominal model
Solar plasma range delay (5 day time constant)	100 % of nominal model
Doppler bias coefficient (15 day time constant)	.01 rpm
<u>Consider Parameters</u>	
DSN station locations (27x27 correlated covariance)	30 cm, each component
Ionosphere zenith delay calibration error	day: 75 cm night: 15 cm
Troposphere zenith delay calibration error	5 cm

The estimation algorithm used to obtain these results was a batch-sequential, square-root information filter, which allows estimated constant and stochastic parameters and unmodeled consider parameters to be included. The most important stochastic parameter for this data arc was the solar plasma, which had a time constant of 5 days, and a process noise (steady-state uncertainty) of 100 percent. All of the filter parameters and their *a priori* uncertainties are given in Table 1. Once an estimate is obtained, the result is smoothed back over the data arc to obtain smoothed data residuals and statistics, which are an important measure of

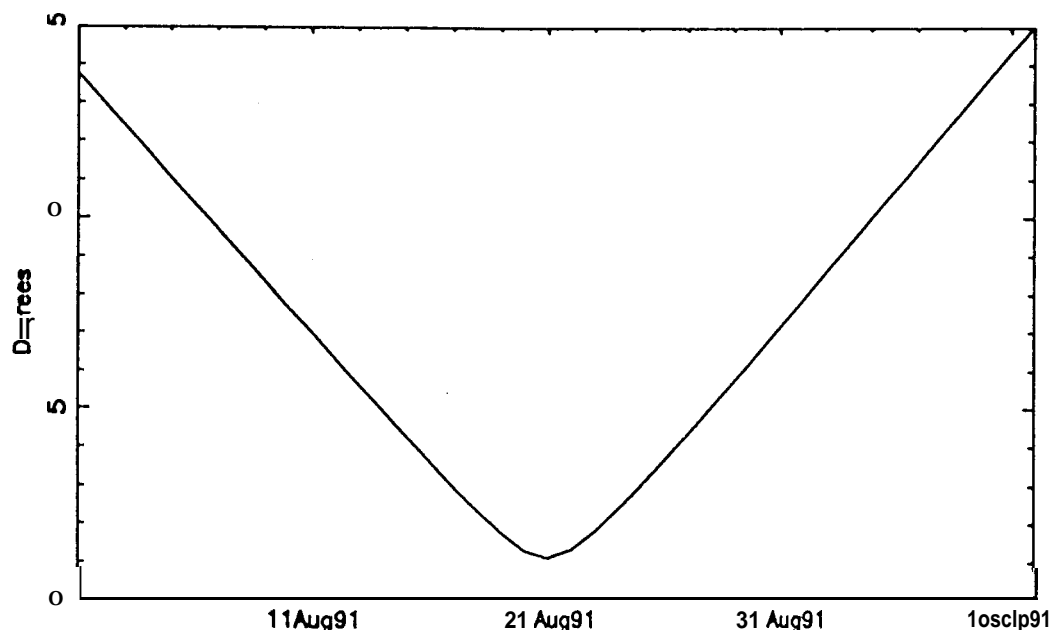


Figure 2 Sun-spacecraft separation angle near conjunction

the quality of the current estimate. During the smoothing process the covariance of the estimate can be obtained at selected points within the data arc, and then transformed to the desired coordinate system. This feature allows estimates at the end of a subset of the data arc to be compared to the estimate obtained from the full data arc at the same epoch, which is also an important evaluation tool.

## RESULTS

### Tracking Data and Data Weights

The data arc used for this study starts on May 21, 1991, when the geocentric Sun-spacecraft separation was 61.1 degrees, and ends September 12, 1991, when the Sun-spacecraft separation was 15.8 degrees. This timespan is largely defined by the S-band data arc, which extends from May 22 to September 5, while the X-band data arc extends to the ends of this timespan and covers most of the region in between. The S-band data have much more substantial gaps during this time, due largely to the operational difficulties encountered when using the S-band transmitter on the spacecraft. Conjunction occurred on August 21, 1991, with a minimum Sun-spacecraft separation of 1.1 degrees. The history of the Sun-spacecraft separation angle is plotted in Figure 2 for the 40 days closest to conjunction. Valid ranging data were obtained down to 1.4 degrees before conjunction, and resumed at 1.7 degrees on the other side, although the last 0.4 degrees of ranging data on each side of conjunction were not used in this study. Interestingly, the loss of S-band ranging data was within 5 to 6 hours of the loss of X-band ranging data close to conjunction, probably due to the S-band uplink employed for both types of ranging data. The nominal solar plasma range delay (based on Eqs. (4) and (5) above) for the data used in this study reaches a maximum of just over 1000 meters for S-band

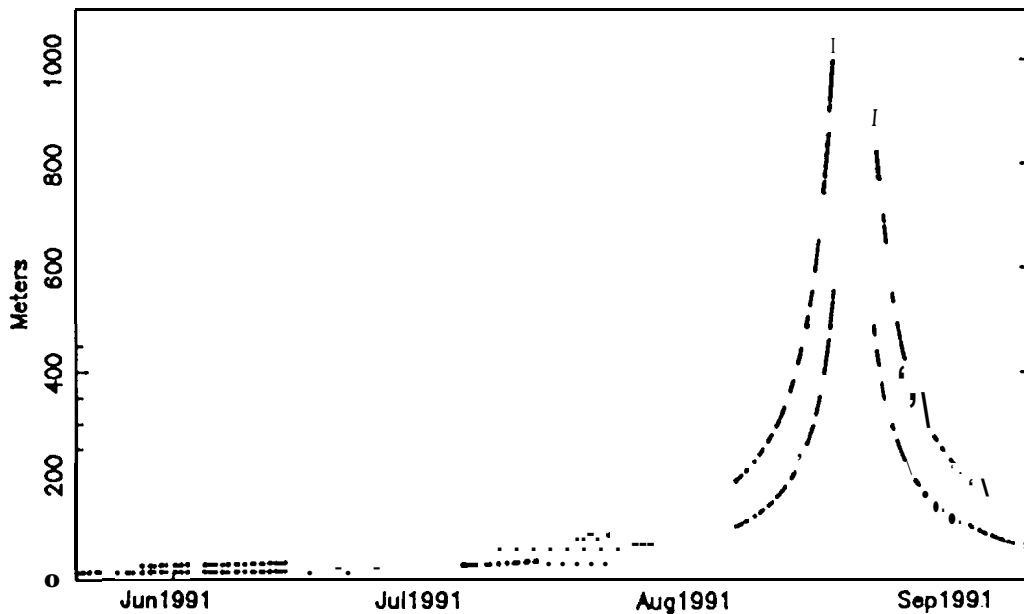


Figure 3 Nominal solar plasma range delay. Upper line is S-band delay, lower line is X-band delay. Values plotted at times of actual range points.

ranging data, and a maximum of about 500 meters for X-band ranging data, as shown in Figure 3. The difference in coverage between the S-band data (the upper line in Figure 3) and X-band data (the lower line) can also be seen for the whole data arc. The behavior of the Doppler data during the approach to conjunction was similar, but the increasing levels of noise before conjunction rendered the data unusable about 3.7 degrees from the Sun. After conjunction the Doppler data were recovered at about the same time as the ranging data,

The technique used to evaluate the new solar plasma delay model was to calculate and then compare three different solutions, consisting of a combined S/S- and S/X-band solution, a S/X-band only solution, and finally a S/S-band only solution. (Note that the "combined" solution is the only one with dual-band data, and will be referred to as the "dual-band" solution, while the "S/X-band" solution has only single-band data, even though the uplink and downlink frequencies are different. ) Due to the difference in the magnitude of the charged particle delay (primarily due to solar plasma, but also including any residual ionosphere calibration errors) between S- and X-band ranging data, the dual-band solution would be expected to exhibit the best navigation performance, as most of the solar plasma effects should be calibrated directly by the ranging data. However, most spacecraft missions currently in the planning stages intend to use only X/X-band tracking systems, and so the quality of the single-band solutions (and particularly of the S/X-band only solution) are important in evaluating the solar plasma model and this technique.

The data weight (*ie.* the assumed  $1\sigma$  accuracy) of the range data was set close to the  $1\sigma$  data noise, which in the case of the X-band data was just under 2 meters for most of the data arc, a result consistent with those obtained earlier (Refs. 1-4). For

the dual-band solution the S/S-band ranging data were deweighted from its noise level to 10 meters to account for differences in the X- and S-band ground station delay calibrations. For both bands the ranging data was deweighted somewhat more aggressively within 7.5 degrees on the incoming side and 8.7 degrees on the outgoing side, to 20 and 30 meters for X- and S-band respectively, with the time spans determined more by data quality than anything else. Starting at 3.7 degrees on the incoming side, the X- and S-band ranging data were further deweighted to 300 and 500 meters, while on the outgoing side the data quality was good enough not to require such measures. The Doppler data were nominally weighted at 1 mm/sec, but there were enough time spans with excessive noise that most of the Doppler data for both bands was deweighted to be consistent with the observed residual scatter. The dual-band solution did not use the S/S-band Doppler data at all, depending instead on the S/X-band Doppler and both ranging data types. The S/X-band solution used S/X-band ranging and Doppler data, while the S/S-band solution used S/S-band ranging ranging (with a 5 meter data weight) and the S/S-band Doppler data.

### **Post-fit Residuals and Estimated Solar Plasma Model Corrections**

The first measure of the validity of a solution is the quality of the fit to the data. The post-fit range residuals and the  $3\sigma$  range data weights of the dual-band solution are shown in Figures 4-7. Figures 4 and 5 show the X- and S-band range residuals for about the first two months of the data arc. While the X-band residuals fit better than the S-band residuals, both data sets are statistically respectable. Figures 6 and 7 show the X- and S-band range residuals from the 40 days around conjunction. The deterioration of the data (and their corresponding clweighting) as the spacecraft approached conjunction can be clearly seen. Still, none of the passes are badly biased, and there are no large trends running through the data. It is also interesting to note that the S/X- and S/S-band range data show a similar noise structure near conjunction, although with a difference in scale. The fit to the S/X-band ranging data for the S/X-band solution is not noticeably different from residuals of the dual-band solution shown in Figures 4 and 6. The ranging residuals from the S/S-band solution are about 1 m less noisy than the dual-band solution at 4 meters (during the first 2.5 months), which is consistent with the data weight, but the ranging residual plots for the S/S-band case appear essentially the same as those shown in Figures 5 and 7.

The Doppler data residuals can be used to validate the level of solar plasma activity, which is expected to be correlated with the mean solar plasma delay. Consequently, the estimated corrections and  $1\sigma$  error bars of the solar plasma model from the dual-band solution are shown in Figure 8, and the S/X- and S/S-band Doppler residuals and  $3\sigma$  weights are shown below it in Figures 9 and 10, respectively. The S/S-band Doppler residuals are necessarily from the S/S-band solution, while the S/X-band Doppler residuals are from the dual-band solution. (The Doppler residuals from the S/X-band solution are not noticeably different from those shown here).

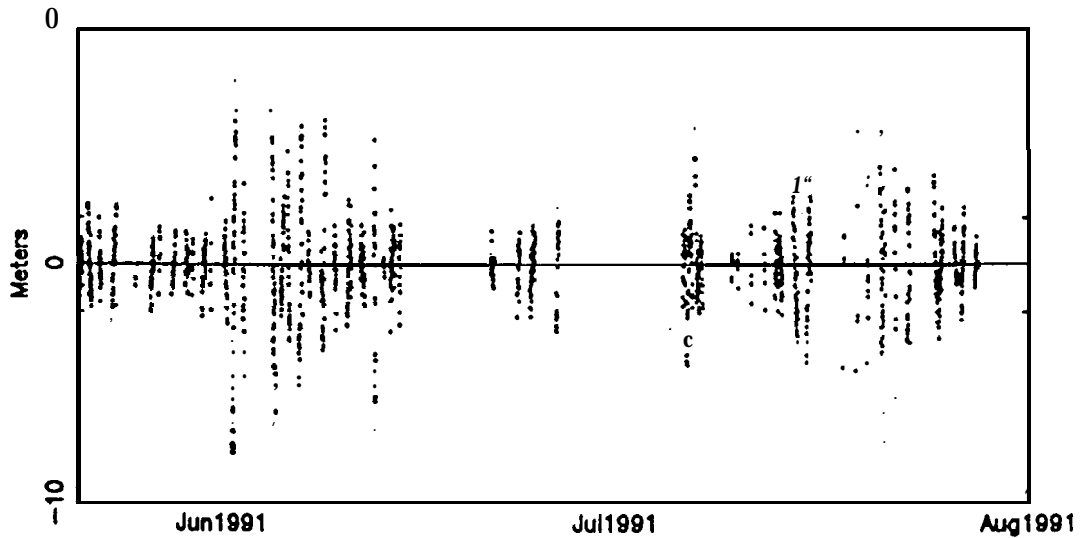


**Figure 4 S/X-band range residuals, first two months.**

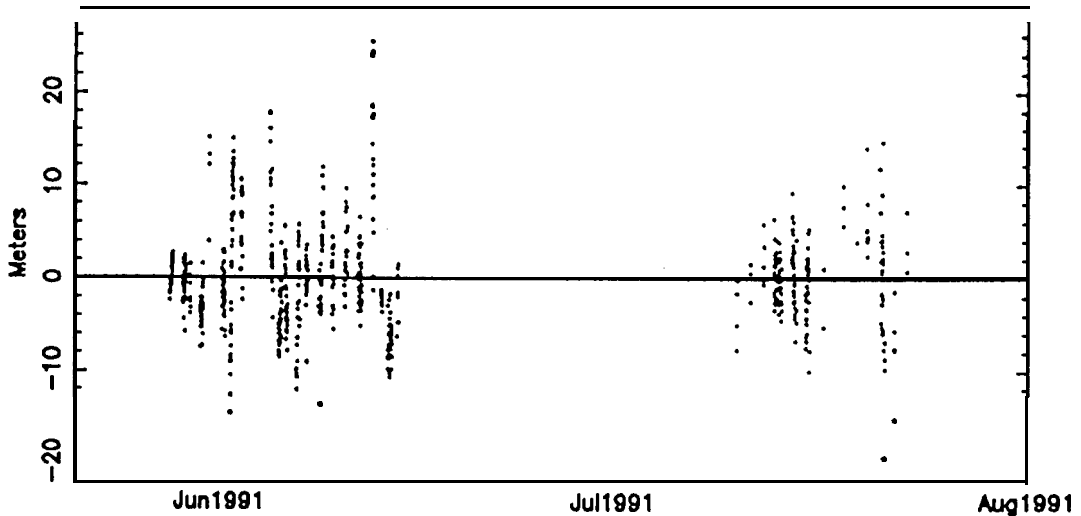


**Figure 5 S/S-band range residuals, first two months.**

Note that before August several regions of increased Doppler noise are matched by estimates of positive increases in the solar plasma delay. While there are two estimates of unrealistic solar plasma values that are under  $-100$  percent (*ie.* negative delay), they occur in regions where the total solar plasma delay is barely over 10 meters at S/X-band, and so they are easily explained by tracking station calibration errors of the same magnitude. Overall, an *a priori* uncertainty of 100 percent in the solar plasma model seemed to produce the best results, even with these occasional errant values, and is consistent with the results reported in Ref. 5.

The solar plasma estimates and uncertainties for the single-band solutions can be compared to the combined solution to determine how well the single-band data is able to determine the solar plasma delay. The solar plasma estimates and  $1\sigma$  uncertainties for the S/X- and S/S-band only solutions are shown in Figures 11

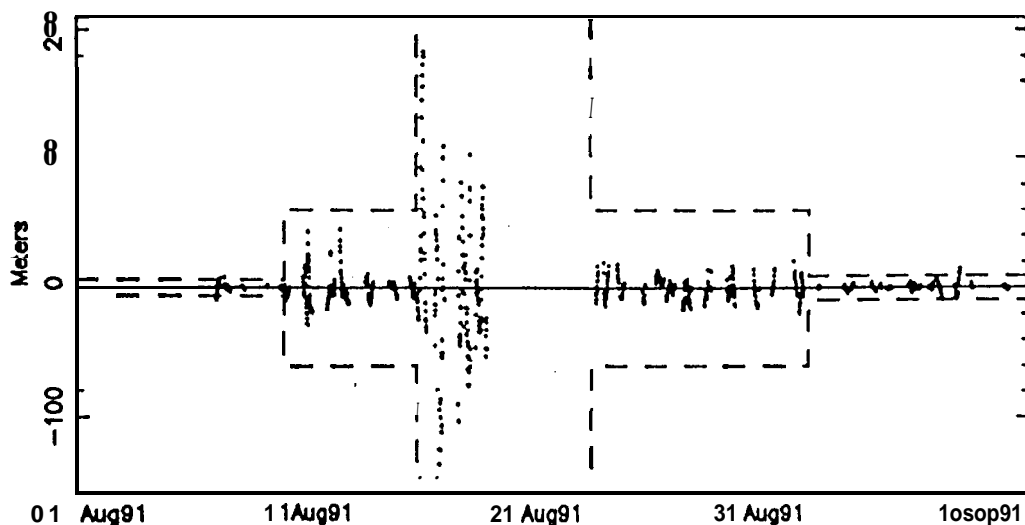


**Figure 6 S/X-band range residuals, near conjunction.**  
Dashed lines are data weights ( $3\sigma$ ).

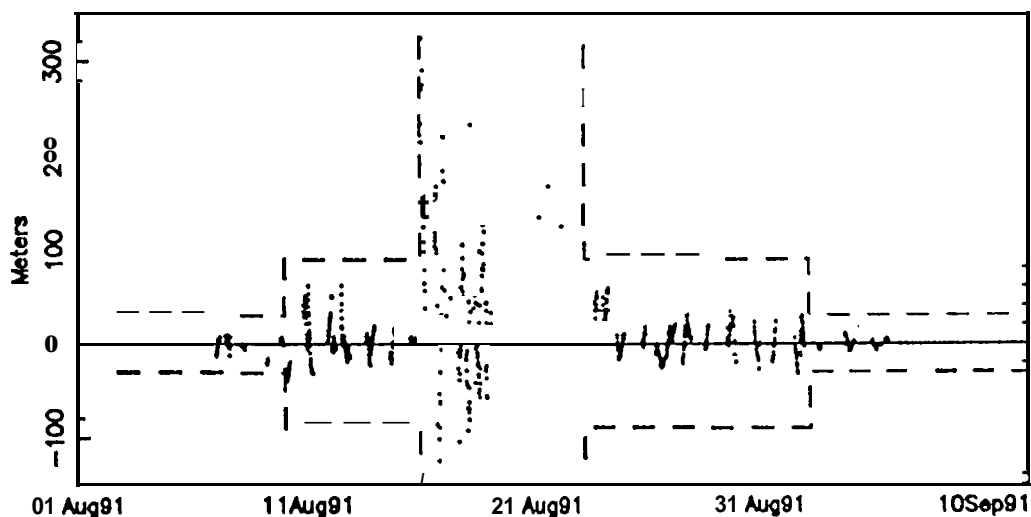


**Figure 7 S/S-band range residuals, near conjunction.**  
Dashed lines are data weights ( $3\sigma$ ).

and 12, respectively, with the dual-band estimates included (as a solid line) for comparison. When comparing the single- and dual-band solutions, it is clear that most of the estimates from both single-band solutions are statistically consistent with the dual-band solution. The S/X-band solution performs better than the S/S-band solution in both consistency and the ability to improve on the 100 percent a priori solar plasma uncertainty, as would be expected. However, even the S/S-band estimates show similar trends to those that are so clearly evident in the dual-band solution.

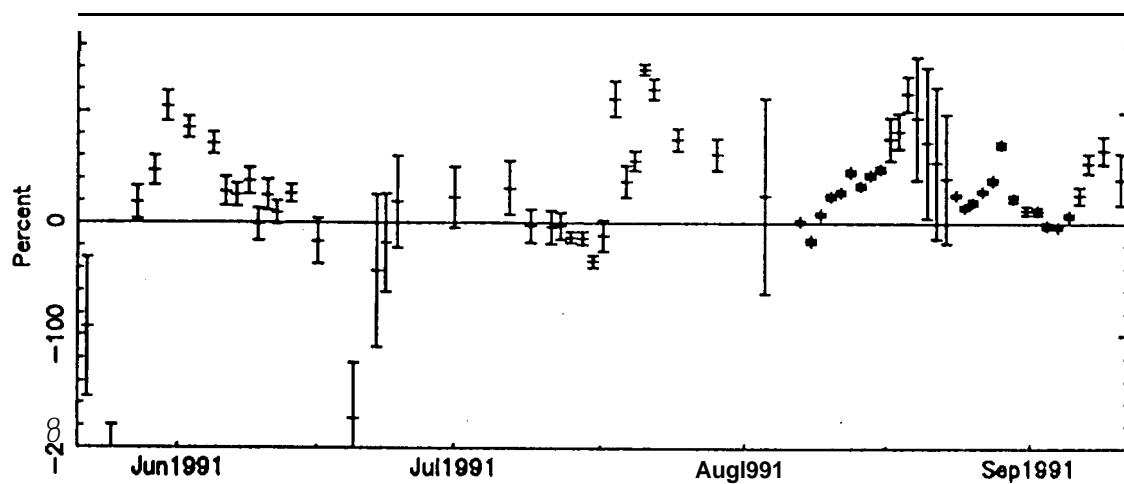


Figure 8 Dual-band solution: solar plasma estimates and error bars ( $1\sigma$ ).

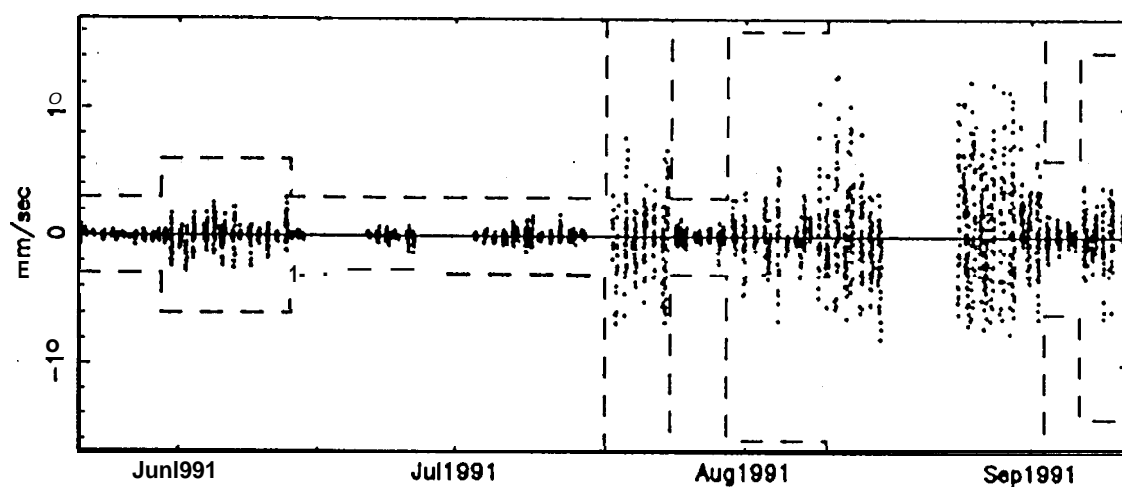


Figure 9 S/X-band Doppler residuals. Dashed lines are data weights ( $3\sigma$ ).

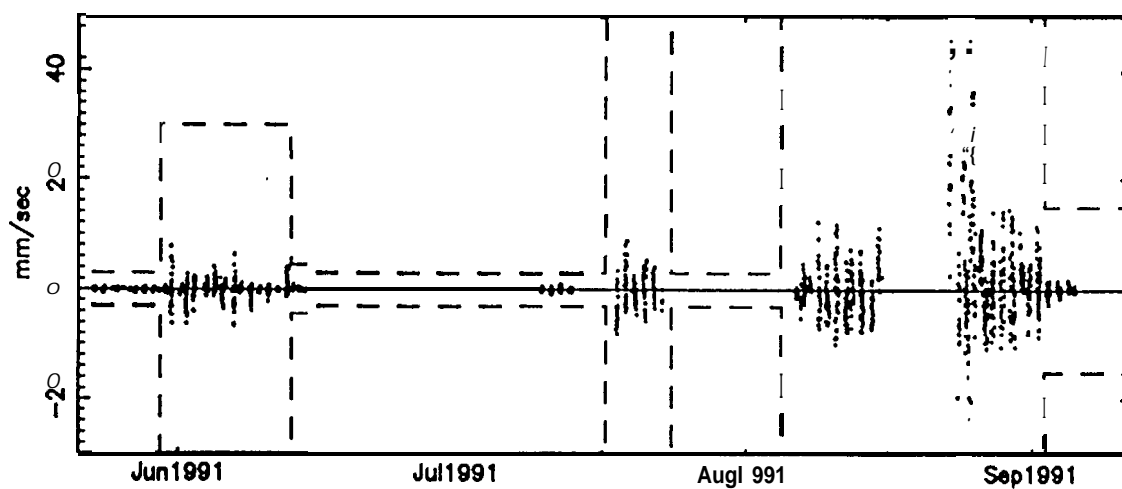
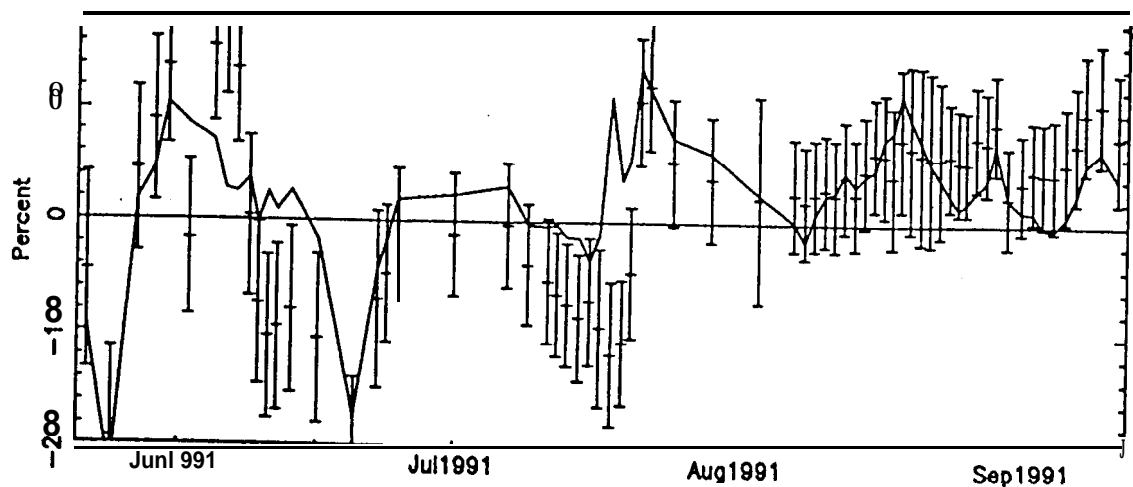
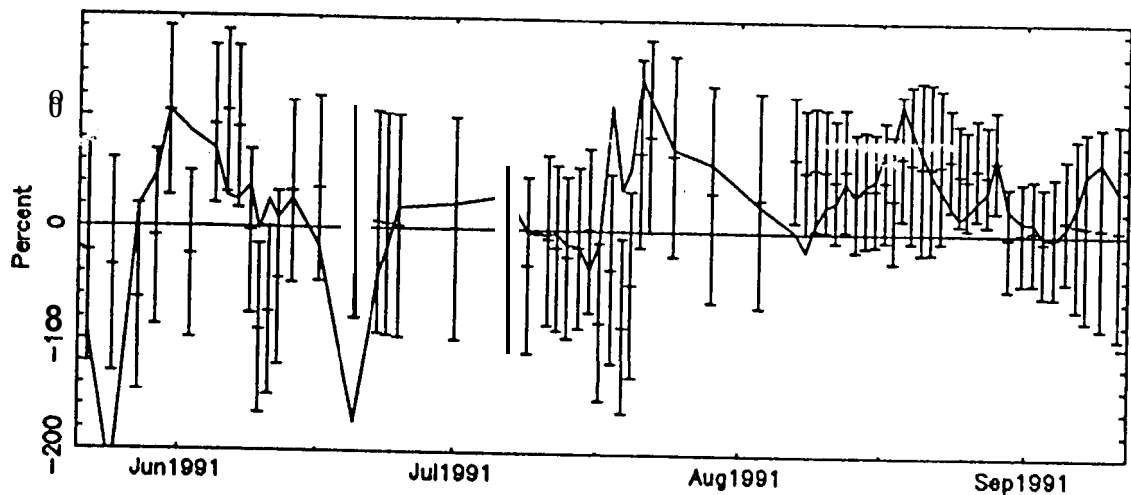


Figure 10 S/S-band Doppler residuals. Dashed lines are data weights ( $3\sigma$ ).



**Figure 11 S/X-band solution: solar plasma model estimates and error bars ( $1\sigma$ ). Solid line is dual-band estimate.**



**Figure 12 S/S-band solution: solar plasma model estimates and error bars ( $1\sigma$ ). Solid line is dual-band estimate.**

## Trajectory Estimate Comparisons

While the effectiveness of this technique in fitting the ranging and Doppler data has been established, the validity of the resulting trajectory estimates still needs to be examined. In order to do this, the dual-band and S/X-band solutions are compared at the end of the data arc with a solution obtained operationally using data from September 12, 1991 to January 8, 1992, which included a significant number of VLBI observations as well as ranging and Doppler data. Because of the VLBI data in this reference solution the geocentric angular error in the resulting reference trajectory is generally no larger than about 50 nanoradians (nrad). The differences in geocentric range, right ascension, and declination between the reference solution and the dual-band and S/X-band solutions, along with the uncertainties of the new solutions, are given in Table 2. While the right ascension difference for the combined

solution is slightly more than the  $1\sigma$  uncertainty, all of the angular differences are statistically consistent to  $1\sigma$  when the 50 nrad uncertainty of the reference solution is taken into account. The range differences are easily explained by noting that the reference solution did not include a solar plasma delay model. The plasma delay at the beginning of the reference solution was about 65 meters, and a ranging data weight of 100 meters was used in the reference solution, so the radial differences in Table 2 have the correct sign and a reasonable magnitude. The S/S-band solution differences are not reported at this epoch (although they will be discussed in the following section) because the S-band data arc ends 6 days earlier, causing the statistics to be unmeaningful due to the rather large *a priori* uncertainties on the precession maneuvers.

**Table 2**  
**COMPARISON OF REFERENCE AND ESTIMATED TRAJECTORIES**

Geocentric Parameter	Dual-band solution		S/X-band solution	
	$\Delta_{REF}$	$\sigma_{EST}$	$\Delta_{REF}$	$\sigma_{EST}$
Range(m)	115	17	139	38
Right Ascension (nrad)	113.2	84	68.9	111
Declination (nrad)	120.2	235	-82.5	278

$A_{REF}$  = reference minus new trajectory

$\sigma_{EST}$  = estimate uncertainty

In addition to establishing the effectiveness of this estimation technique in determining a trajectory solution using data from well beyond both sides of conjunction, it is important to measure the validity of solutions obtained with data cutoffs during the approach to conjunction and sooner afterwards than the end of the data arc described above. For example, the Galileo spacecraft arrives at Jupiter in 1995 with a Sun-spacecraft separation of only 8.6 degrees, which is close to range of separation angles examined here. To obtain comparisons within the data arc, the full-length dual-band solution was smoothed back to the batch containing the time of the desired data cutoff to obtain a trajectory estimate and covariance at that epoch, while the estimate and covariance of the solution to be compared was obtained from only the data up to the cutoff time. Both sets of estimates and covariances were then transformed into geocentric spherical coordinates to provide a more meaningful basis for comparison. Using this method, shorter data arcs from all three solutions were compared at four epochs to the full combined solution. The radial differences and  $1\sigma$  uncertainties of the shorter data arcs, along with the  $10\sigma$  uncertainty of the combined solution, the Sun-spacecraft separation angle, and the epoch are shown in Table 3. In Table 3 there are three epochs on the approach to conjunction, and one afterward. With the exception of the first epoch, all the differences for the shorter data arcs of the dual-band solution are consistent to  $1\sigma$  with the full combined solution. While the difference at the first epoch is large at  $2.5\sigma$ , the magnitude of the error is still small. The S/X-band solutions are all.

consistent to better than  $1\sigma$ , and the S/S-band solutions differ by just over  $1\sigma$  for the epoch closest to conjunction, which is not unexpected.

Table 3  
RADIAL DIFFERENCES(m) FOR SHORT-ARC ESTIMATES

Short-arc Data End	SEP* (deg)	$\sigma_f$	Dual-band		S/X-band		S/S-band	
			$\Delta_f$	$\sigma_s$	$\Delta_f$	$\sigma_s$	$\Delta_f$	$\sigma_s$
11 Aug 01:00	7.0	5	-24.5	9	41.5	84	183.8	217
16 Aug 10:00	3.4	54	-79.0	79	10.9	186	-294.4	337
19 Aug 04:00	1.7	172	34.6	249	-304.5	496	-1010.9	847
02 Sep 07:00	8.8	4	-19.9	13	-29.8	80	-133.2	126

\* Geocentric Sun-spacecraft separation angle  $\sigma_f$  = full solution mapped uncertainty

$\Delta_f$  = full solution minus short-arc estimate  $\sigma_s$  = short-arc estimate uncertainty

The corresponding geocentric angular differences and uncertainties are shown in Tables 4 and 5 for right ascension and declination, respectively. Looking at the angular differences for the dual-band solutions, it can be seen that none of the estimates from the shorter data arcs deviate significantly from the full solution. The S/X-band solutions do have differences of slightly more than  $1\sigma$  for the middle two epochs, but this is not unexpected out of a total of eight angular differences. These differences, and similar (thought smaller)  $1\sigma$  uncertainties, may be taken to put a limit on S/X-band only navigation performance very near the Sun of about 350

Table 4  
RIGHT ASCENSION DIFFERENCES (nrad) FOR SHORT-ARC ESTIMATES

Short-arc Data End	$\sigma_f$	Dual-band		S/X-band		S/S-band	
		$\Delta_f$	$\sigma_s$	$\Delta_f$	$\sigma_s$	$\Delta_f$	$\sigma_s$
11 Aug 01:00	47	-14.8	83	29.7	105	506.7	288
16 Aug 10:00	52	12.2	91	-6.3	114	341.5	274
19 Aug 04:00	55	9.9	97	-8.6	121	352.7	285
02 Sep 07:00	72	25.7	116	65.0	143	481.7	269

nrad in declination and 110 to 145 nrad in right ascension, compared with  $1\sigma$  uncertainties of 125 to 150 nrad declination and 50 nrad in right ascension for more benign Sun-spacecraft separation angles. The S/S-band solutions show rather large uncertainties in declination and fairly significant (at  $2\sigma$ ) deviations in right ascension. The implication of these S/S-band solutions is that the solar plasma model is not fully adequate to produce S/S-band solutions that are statistically consistent to  $1\sigma$ . However, even the S/S-band solutions using this method should be valid this near the Sun to within 500 nrad in right ascension and 900 nrad in declination, should these rather large uncertainties ever be of any use to another spacecraft mission. It is possible that planned improvements to the solar plasma

model will correct these deficiencies in S/S-band solutions and yield more useful results. In summary, when the alternative of deleting all range data within 10 degrees of the Sun is considered, this model works well enough as described here to make a significant contribution to spacecraft navigation for small Sun-spacecraft separation angles.

**Table 5**  
**DECLINATION DIFFERENCES(nrad)FOR SHORT-ARC ESTIMATES**

Short-arc Data End	$\sigma_f$	Dual-band	S/X-band	S/S-band
		A $\sigma_s$	A $\sigma_s$	A $\sigma_s$
11 Aug 01:00	159	-287.9 259	-269.0 299	827.2 706
16 Aug 10:00	169	-164.9 268	-354.2 315	455.5 657
19 Aug 04:00	175	-178.9 281	-366.0 331	469.6 679
02 Sep 07:00	210	-145.7 306	-198.0 368	729.7 617

## CONCLUSIONS

In this paper the development of a simple approximation for the effect of charged particles in the solar plasma on ranging data acquired from interplanetary spacecraft was described. The validity and utility of this model were tested by estimating the solar plasma behavior using S/S-band and S/X-band two-way ranging data acquired from the Ulysses spacecraft as it approached its first solar conjunction in the spring and summer of 1991. The results of these experiments yielded estimates from the different data sets of solar plasma variations along the Earth-spacecraft radio signal path that are statistically consistent with one another. In addition, comparisons of the estimated spacecraft trajectory obtained with the different data sets utilized in the analysis indicate that the trajectory solutions derived with the use of the solar plasma model are also largely consistent with each other within the uncertainties associated with each solution. In summary, these results, coupled with the results of previous demonstrations of accurate ranging, indicate that the combined use of appropriate error models for solar plasma behavior, ground station electronic calibration errors, and spacecraft non gravitational forces in the orbit determination process enable the operational use of highly accurate ranging for interplanetary navigation over almost all tracking geometries.

## ACKNOWLEDGEMENTS

This work was carried out at the Jet Propulsion Laboratory, California Institute of Technology, Pasadena, California, under contract with the National Aeronautics and Space Administration. The authors would like to thank Bill Folkner for his work on the original solar plasma modeling program, and to thank Jordan Ellis for the helpful insights shared by him during the preparation of this paper.

## REFERENCES

1. Thurman, S. W., McElrath, T. P., Pollmeier, V. M. "Short-arc Orbit Determination using Coherent X-band Ranging Data", AAS/AIAA Spaceflight Mechanics Meeting, AAS 92-109, 24-26 February 1992.
2. Pollmeier, V. M., and Thurman, S. W. "Application of High Precision Two-way Ranging to Galileo Earth-1 Encounter Navigation", *The Telecommunications and Data Acquisition Progress Report 42-11 O*, Vol. April-June 1992, 15 August 1992.
3. McElrath, T. P., Tucker, B., Criddle, K. E., Menon, P. R., Higa, E. S. "Ulysses Navigation at Jupiter Encounter", AIAA/AAS Astrodynamics Conference, AIAA 92-4524, 10-12 August 1992.
4. Pollmeier, V. M., Kallemeyn, P. H., and Thurman, S. W. "Application of High Precision Two-way S-Band Ranging to the Navigation of the Galileo Earth Encounters", AAS/GSFC International Symposium on Space Flight Dynamics, AAS 93-251, 26-30 April 1993.
5. Coles, W. A., and Harmon, J. K. "Propagation Observations of the Solar Winds Near the Sun", *Astrophysical Journal* 337, pp. 1023-1034, 15 February 1989. "
6. Efron, L., and Lisowski, R. J. "Charged Particle Effects to Radio Ranging and Doppler Tracking Signals in a Radially Outflowing Solar Wind", *JPL Space Programs Summary 37-56*, Vol. 2, January-February 1969.